arXiv:1611.01637v1 [astro-ph.SR] 5 Nov 2016

Chemical analysis of a carbon-enhanced very metal-poor star: CD−27 14351

Drisya Karinkuzhi[1]

1 - Indian Institute of Astrophysics, Koramangala, Bangalore 560034

and

Aruna Goswami[1],

1 - Indian Institute of Astrophysics, Koramangala, Bangalore 560034

and

Thomas Masseron[2],

2 - Institute of Astronomy, Madingley Road, Cambridge CB3 0HA, UK

ABSTRACT

We present the first time abundance analysis of a very metal-poor carbon-enhanced star CD−27 14351 based on a high resolution (R ∼ 48 000) FEROS spectrum. Our abundance analysis performed using Local Thermodynamic Equilibrium (LTE) model atmospheres shows that the object is a cool star with stellar atmospheric parameters, effective temperature T_{eff} = 4335 K, surface gravity log g = 0.5, microturbulence ξ = 2.42 km s^{-1}, and, metallicity [Fe/H] = −2.6. The star exhibits high carbon and nitrogen abundances with [C/Fe] = 2.89 and [N/Fe] = 1.89. Overabundances of neutron-capture elements are evident in Ba, La, Ce, and Nd with estimated [X/Fe] > 1, the largest enhancement being seen in Ce with [Ce/Fe] = 2.63. While the first peak s-process elements Sr and Y are found to be enhanced with respect to Fe, ([Sr/Fe] = 1.73 and [Y/Fe] = 1.91) the third peak s-process element Pb could not be detected in our spectrum at the given resolution. Europium, primarily a r-process element also shows an enhancement with [Eu/Fe] = 1.65. With [Ba/Eu] = 0.12 the object CD−27 14351 satisfies the classification criterion for CEMP-r/s star. The elemental abundance distributions observed in this star is discussed in light of chemical abundances observed in other CEMP stars from literature.

Subject headings: stars: carbon —- stars: chemically peculiar—- stars: late-type —- stars: low-mass

1. INTRODUCTION

The object CD−27 14351 drew our attention when a low-resolution spectrum of this object acquired on Oct 23, 2015, during the observing run of our observational program with HCT (Himalayan Chandra Telescope, at IAO, Hanle; one of the objectives of this program is to search for CH stars and carbon-enhanced metal-poor stars among field stars) on visual inspection was found to show significant resemblances with the low-resolution spectrum of HD 5223, a well-known classical CH star. From the known stellar parameters of HD 5223, (T_{eff} = 4500 K, log g = 1.0 and metallicity [Fe/H] = −2.06 (Goswami et al. 2006), a first guess was the object CD−27 14351 could also be a cool metal-poor object similar to HD 5223. Dominant carbon bearing molecular bands in its spectrum also indicated that the object is likely carbon-enhanced. For an understanding of its elemental abundance pattern and its origin, a detailed chemical composition study was taken up based on a high resolution FEROS (Fiber-fed Extended Range Optical Spectrograph, connected to the 1.52 m telescope at Chile) spectrum.

Our analysis reveal that the object is indeed a carbon-enhanced metal-poor star that also show significant enhancement of nitrogen and neutron-capture elements. The heavy elements abundance estimates indicate that the surface composition of the object has significant contributions originated from both the r-process as well as the s-process nucleosynthesis. This is supported by our estimate of the abundance ratio [Ba/Eu] (=0.12), that qualifies the object to be placed in the CEMP-r/s group (Beers & Christlieb (2005), for definition of CEMP-r/s stars and other CEMP stars). However, the origin of CEMP-r/s stars still remains far from clearly understood. Several proposed physical scenarios are available in literature (Qian & Wasserburg 2003; Zijlstra 2004; Barbuy et al. 2005; Wanajo et al. 2006). In spite of considerable efforts no single mechanism has yet been identified that could explain satisfactorily the production of enhanced carbon and heavy-element abundance patterns observed in the group of these stars. While the enhancement in the s-process elements is believed to be due to mass transfer in binary systems involving AGB companion that underwent s-process nucleosynthesis, the origin of the enhanced abundance of the r-process element Eu remains unexplained in this scenario. In a recent work Hampel et al. (2016) have shown that the observed abundance patterns of CEMP-r/s stars could be convincingly reproduced through i-process (intermediate neutron-capture process) which operates at neutron densities between those of the s-process and r-process. Except for one object the abundance patterns of all the stars in their sample could be reproduced by this process. To place observational constraints on the nucleosynthesis of s-, r- and i-process elements at low metallicity, it is necessary to conduct high-resolution spectroscopic analysis of stars with excess of heavy elements and CEMP stars undoubtedly form important targets. Such studies would help provide insight into the possible origin of these classes of objects. Our detailed high resolution spectroscopic analysis of CD−27 14351 is prompted by such motivations.

In Section 2, we describe the source of the low-resolution and high resolution spectra of the programme star. In section 3 we present our estimates of effective temperatures based on available BVJHK photometry of the object. The spectral analysis procedures and estimation of the stellar atmospheric parameters are discussed in Section 4. The elemental abundance results and discussions are presented in Section 5. Uncertainty in elemental abundances are discussed in section 6. Conclusions are provided in Section 7.

2. Spectra of CD−27 14351

The low-resolution spectrum of CD−27 14351 was acquired on October 23, 2015, using HFOSC attached to the 2-m HCT (Himalayan Chandra Telescope) at the Indian Astronomical Observatory (IAO), Mt Saraswati, Digpa-ratsa Ri, Hanle. The spectrograph used is HFOSC (Himalayan Faint Object Spectrograph Camera). The spectrum covers the wavelength range 3800 - 6800 Å at a resolution R ∼ 1300. The high resolution FEROS (FEROS: the Fiber-fed Extended Range Optical Spectrograph, connected to the 1.52 m telescope at ESO, Chile) spectrum of CD−27 14351 used in this study was acquired on July 14, 2000, has a resolution of R ∼ 48000 and covers the wavelength range spanning 3500 - 9000 Å . The estimated radial velocity is ∼ 61.1 km s^{-1}. The basic data for this object is listed in table 1.

3. Temperatures from photometric data

We have calculated the photometric temperatures of CD−27 14351 using the temperature calibrations of Alonso et al. (1999, 2001) for the giants. The estimated values along with the spectroscopic temperature estimate are given in table 2. As can be seen in the following section the derived spectroscopic temperatures are higher by ≈ 300 K from J - K and J - H temperatures and ≈ 400 K from the V - K temperatures. This discrepancy is probably due to the high carbon enhancement that changes significantly the colours; due to the severe blending from the molecular lines B - V temperatures could be much lower than the spectroscopic temperature estimate.

Table 1: Basic data for the program stars

Star Name.	RA(2000)	DEC(2000)	B	V	J	H	K
CD−27 14351	19 53 08.00	-27 28 14.96	11.82	9.70	7.022	6.296	6.135

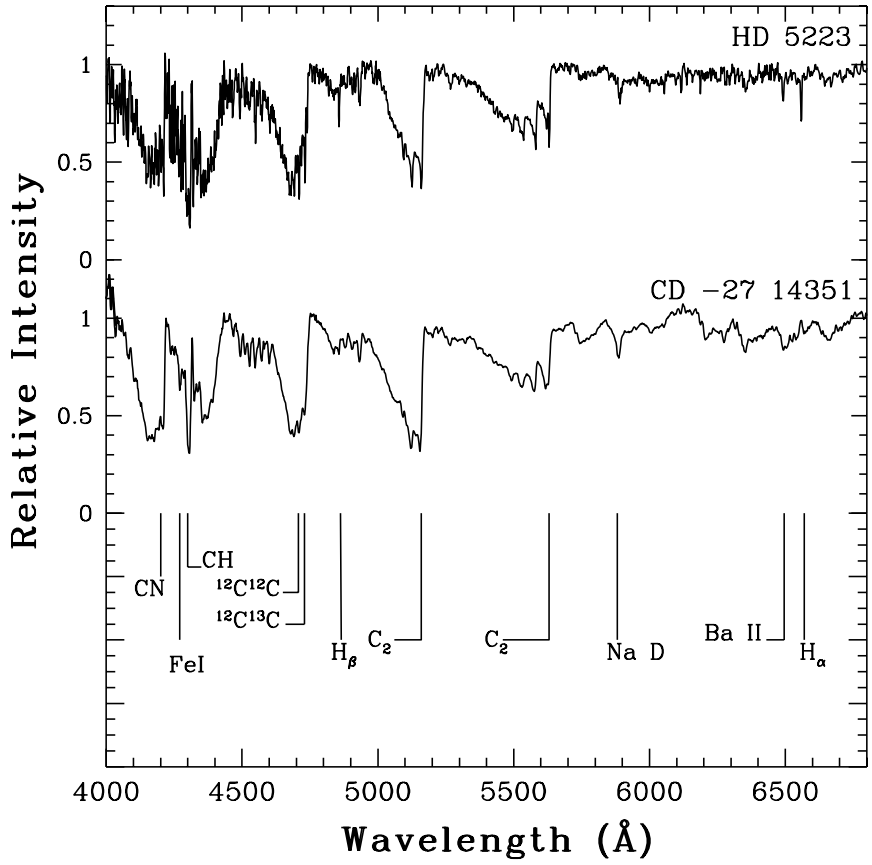

Fig. 1.— A comparison of the low resolution spectrum of CD−27 14351 with the spectrum of CH star HD 5223. Some prominent features are indicated in the figure.

Table 2: Temperatures from photometry

Star Name	T_{eff} (J - K) K	T_{eff}(J - H) K	T_{eff} (V - K) K	T_{eff} (B - V) K	Spectroscopic K
CD−27 14351	4067	4026 (-2.0)	3900 (-2.0)	2635(-2.0)	4335
		3989(-2.5)	3900 (-2.5)	2528(-2.5)	
		3938(-3.0)	3904 (-3.0)	2438(-3.0)	

The numbers in the parenthesis indicate the metallicity values at which the temperatures are calculated.

4. Spectral analysis

In figure 1, we show a comparison of the spectrum of CD − 27 14351 with the spectrum of the classical CH star HD 5223 (Goswami 2005) obtained from the same observational set up. The spectra of these two objects distinctly show close resemblances with each other. The high resolution FEROS spectrum is used for determination of stellar atmospheric parameters and elemental abundances. The stellar parameters are determined by measuring the equivalent widths of clean unblended Fe I and Fe II lines. The spectrum of CD−27 14351 is severely blended with contributions from carbon molecular bands throughout the spectrum making it difficult to find clean unblended lines of Fe I and Fe II. Only seventeen lines of Fe I and two lines of Fe II are found usable for deriving the stellar atmospheric parameters. Lines with excitation potential in the range 0.0 eV to 5.0 eV and equivalent width 20 Å to 160 Å are selected for this purpose. These lines along with the abundances derived from each line computed using the latest version of MOOG (Sneden 1973) are listed in table 3. We have used the Kurucz grid of model atmospheres with no convective overshooting (http: //cfaku5.cfa.harvard.edu/) and assumed LTE condition throughout the analysis. The method of excitation equilibrium is used for deriving the effective temperature T_{eff}. The initial value is assumed to be the photometric temperatures and the finally adopted value is obtained by an iterative process until the slope of the abundance versus excitation potential of Fe I lines is found to be nearly zero (Figure 2, lower panel). The microturbulent velocity is fixed at this temperature by demanding that there be no dependence of the derived Fe I abundance on the equivalent widths of the corresponding lines (Figure 2, upper panel). The surface gravity is fixed at a value which makes the abundances of iron from the Fe I and Fe II lines equal. The adopted stellar parameters are listed in table 4.

5. Results and discussions: elemental abundances

Elemental abundances are derived from the measured equivalent widths of lines due to neutral and ionized elements if clean unblended lines are present. We have also performed spectral synthesis calculations to derive the elemental abundances for a few elements considering the hyperfine splitting effects. These elemental abundances along with the abundance ratios with respect to iron are presented in table 5. We have also calculated the [ls/Fe], [hs/Fe] and [hs/ls] values, where ls represents light s-process elements Sr and Y and hs represents heavy s-process elements Ba, La, Ce, and Nd. These estimates are presented in table 6.

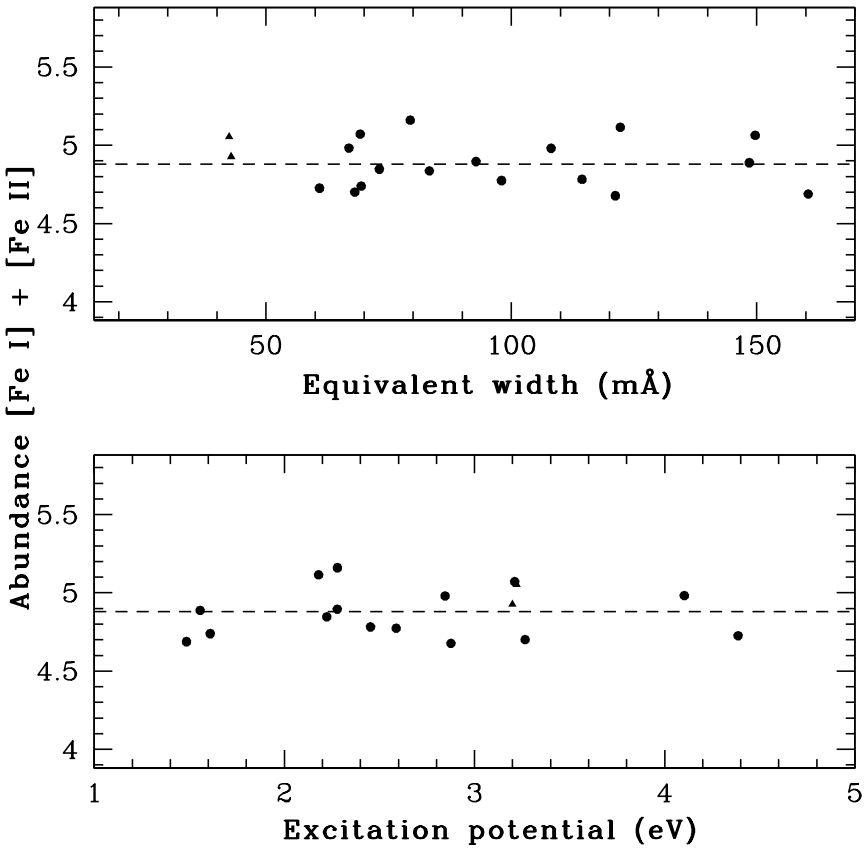

Fig. 2.— The iron abundance of CD−27 14351 is shown for individual Fe I (solid circles) and Fe II (solid triangles) lines as a function of excitation potential (lower panel) and as a function of equivalent width (upper panel).

Table 3. Lines used for the analysis

Wavelength Å	Element	E_{low} ev	log gf	Equivalent width (mÅ)	log ϵ dex	Reference
5688.220	Na I	2.104	-0.45	58.3	4.89	1
4571.100	Mg I	0.000	-5.69	154.1	5.88	2
5528.405		4.350	-0.62	61.1	5.04	3
5172.680		2.710	-0.40	304.7	5.92	4
5261.710	Ca I	2.521	-0.73	27.1	4.39	5
6439.070		2.530	0.47	109.6	4.42	5
6499.650		2.523	-0.59	65.2	4.72	5
4999.500	Ti I	0.830	0.25	134.0	3.33	6
5210.390		0.048	-0.88	120.6	3.04	6
5192.970		0.020	-1.01	143.1	3.38	6
4443.790	Ti II	1.080	-0.70	178.7	3.29	6
4589.950		1.236	-1.79	94.9	3.02	6
5226.530		1.570	-1.30	131.9	3.30	6
5247.570	Cr I	0.961	-1.64	29.0	2.95	6
5348.312		1.003	-1.29	33.0	2.72	6
4476.019	Fe I	2.845	-0.57	108.1	4.98	7
4890.755		2.876	-0.43	121.2	4.68	8
4924.770		2.279	-2.22	79.4	5.16	8
4982.524		4.103	0.14	66.9	4.99	9
4994.130		0.915	-3.08	149.7	5.06	8
5171.600		1.485	-1.79	160.5	4.69	8
5194.941		1.557	-2.09	148.5	4.89	8
5198.711		2.223	-2.14	73.1	4.85	8
5202.340		2.180	-1.84	122.2	5.12	8
5217.389		3.211	-1.10	69.2	5.07	9
5247.050		0.087	-4.98	83.3	4.84	8
5307.370		1.610	-2.98	69.4	4.74	8
5339.928		3.266	-0.68	68.1	4.70	8
5415.192		4.386	0.50	60.9	4.73	8
6137.694		2.588	-1.40	98.0	4.77	8
6136.615		2.453	-1.40	114.4	4.78	8
6421.350		2.278	-2.03	92.8	4.90	8
5234.625	Fe II	3.22	-2.05	38.5	4.97	8
5276.002		3.199	-1.90	40.5	4.88	8

Table 3 (cont.): Lines used for the analysis

Wavelength Å	Element	E_{low} ev	log gf	Equivalent width (m Å)	log ϵ dex	References
4607.327*	Sr I	0.000	-0.57	43.9	2.02	10
5289.815*	Y II	1.033	-1.85	70.4	1.52	11
5662.925		1.944	0.16	135.5	1.74	12
4934.076	Ba II	0.000	-0.15	414.6	1.38	5
6141.713*		0.704	-0.08	287.2	1.34	5
6496.897		0.604	-0.38	298.0	1.47	5
4526.111	La II	0.772	-0.77	60.1	0.49	13
4921.776*		0.244	-0.68	94.6	0.09	14
4460.207	Ce II	0.477	0.17	146.3	1.49	15
4527.348		0.320	-0.46	144.3	1.79	15
4451.981	Nd II	0.000	-1.34	38.3	0.10	16
4811.342		0.063	-1.14	50.9	0.07	16
5212.361*		0.204	-0.87	61.5	0.04	16
5293.163		0.823	-0.00	71.7	0.22	17
6645.064*	Eu II	1.380	0.20	synth	-0.40	18

*Abundances are also derived by spectral synthesis calculations of these lines. The results are presented in Table 5.

1. Kurucz & Peytremann (1975), 2. Laughlin & Victor (1974), 3. Lincke & Ziegenbein (1971), 4. Anderson et al. (1967), 5. Miles & Wiese (1969), 6. Martin et al. (1988), 7. Bridges & Kornblith (1974), 8. Fuhr et al. (1988), 9. Kurucz (1988), 10. Corliss & Bozman (1962), 11. Hannaford et al. (1982), 12. Cowley & Corliss (1983), 13. Andersen & Petkov (1975), 14. Corliss & Bozman (1962), 15. McEachran & Cohen (1971), 16. Meggers et al. (1975) 17. Ward et al. (1985), 18. Biemont et al. (1982)

Table 4: Derived atmospheric parameters of CD−27 14351

Star Name.	T_{eff} K	log g	ξ km s^{-1}	[Fe I/H]	[Fe II/H]
CD−27 1435	4335	0.5	2.42	−2.62	−2.57

5.1. Carbon, Nitrogen, Oxygen

Several strong molecular features of carbon are clearly noticeable throughout the spectrum of CD−27 14351. We have calculated the carbon abundance from the spectral synthesis of C_2 band at 5635 Å (figure 3, middle panel). The C_2 band at 5165 Å is found to be saturated. Carbon shows a large enhancement with [C/Fe] value of 2.89 as estimated from the C_2 molecular band at 5635 Å . Abundance of carbon derived from the CH band at 4300 Å (figure 3, lower panel) also shows similar value with [C/Fe] = 2.88. For the line lists of CH, C_2, CN and $^{12}C^{13}C$ we have consulted Masseron et al. (2014); Brooke et al. (2013); Sneden et al. (2014) and Ram et al. (2014). Using the estimated carbon abundance, nitrogen abundance was derived from spectral synthesis calculation of CN band with band head at 4215 Å (figure 4). Estimated nitrogen abundance ∼ 7.1 dex gives [C/N] = 1.0 for this object. We could not detect any oxygen lines in the spectrum due to severe distortion in the spectrum. We have estimated the $^{12}C/^{13}C$ ratio from the ^{12}CN and ^{13}CN features near 8005 Å (figure 3, top panel). Estimated $^{12}C/^{13}C$ = 10.1 for this object. Such a low value is not unreasonable as the estimated log g value of CD−27 14351 indicates that the object is an evolved red giant star in which the CN cycled materials are expected to mix up into the atmosphere making the $^{12}C/^{13}C$ ratio low.

5.2. Sodium (Na) and Aluminum (Al)

We have derived the Na abundance from Na I line at 5688.22 Å . Estimated Na abundance is high with [Na/Fe] = 1.27. Since this line is free from NLTE effects (Baumueller & Gehren 1997) we have not applied NLTE correction to the derived abundance. A few very metal-poor stars are also known to show such high abundances of Na (Aoki et al. 2002b,a, 2007, 2008). Abundance of Al could not be estimated in CD−27 14351.

5.3. Abundances of α- elements

We have estimated [Mg/Fe] ∼ 0.64 from three Mg I lines at 4571.1, 5172.68 and 5528.41 Å . This value is slightly higher than the general trend of [α/Fe] = 0.4 noticed in metal-poor stars. We have measured three clean Ca I lines in the spectrum of CD−27 14351. Similar to Mg, calcium also shows large enhancement with [Ca/Fe] value 0.79. Ti shows enhancement with [Ti I/Fe] and [Ti II/Fe] values 0.92 and 0.83 respectively. Johnson (2002) have also found that Ti I and Ti II are discrepant in metal-poor stars, likely because of NLTE effects. These estimates show that the object is a very metal-poor star with high abundances of α elements.

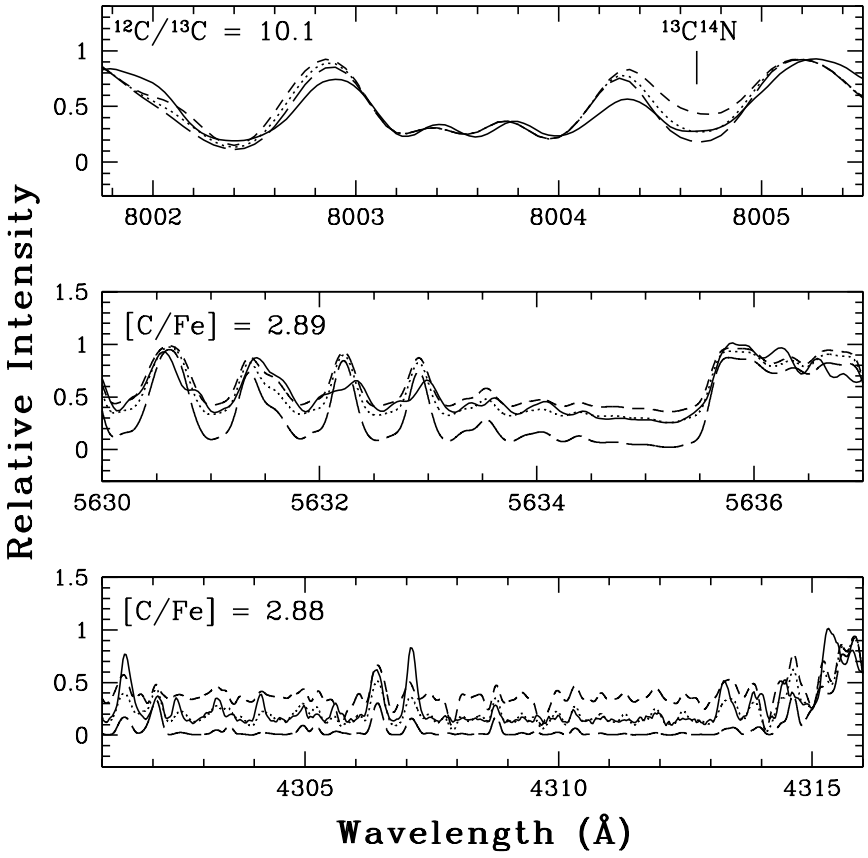

Fig. 3.— Lower panel: The spectral synthesis fits of the CH feature around 4315 Å . Middle panel: The spectral synthesis of C_2 band around 5635 Å . In both the panels the dotted lines indicate the synthesized spectra and the solid lines indicate the observed line profiles. Two alternative synthetic spectra for [C/Fe] = +0.3 (long-dashed line) and [C/Fe] = −0.3 (short-dashed line) are shown to demonstrate the sensitivity of the line strength to the abundances. Top panel: The spectral synthesis fits of the CN features around 8005 Å obtained with the adopted N abundance and $^{12}C/^{13}C \sim 10.1$ (dotted curve). The observed spectrum is shown by a solid curve. Two alternative fits with $^{12}C/^{13}C \sim 25$ (short-dashed line) and 5 (long-dashed line) are shown to illustrate the sensitivity of the line strengths to the isotopic carbon abundance ratios.

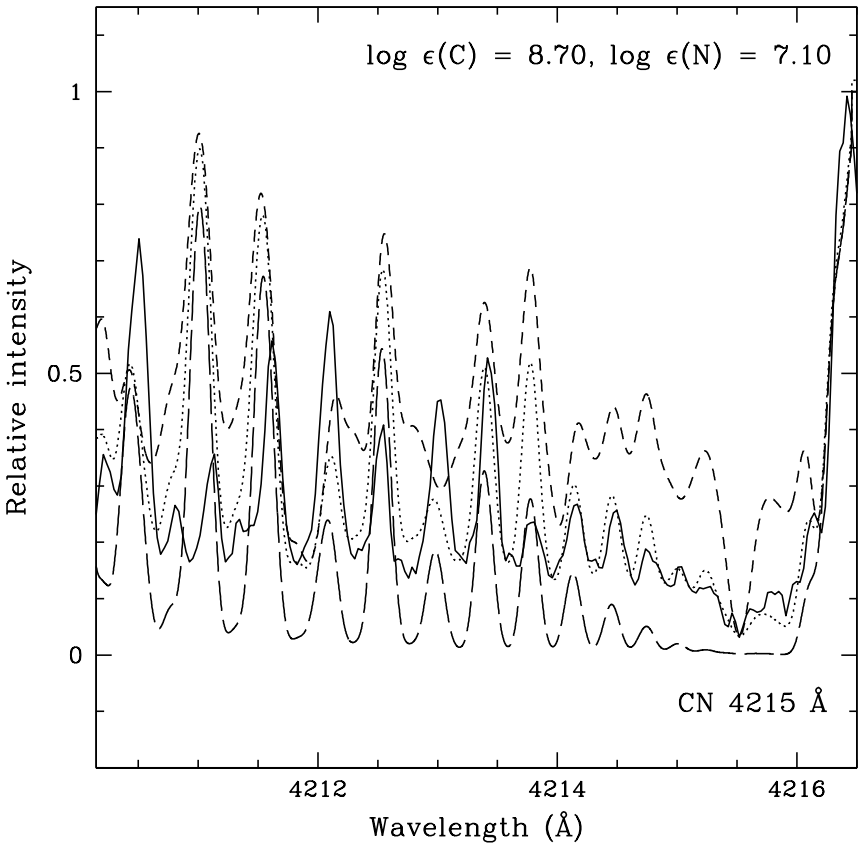

Fig. 4.— Spectral synthesis fits of CN band around 4215 Å . The best fit obtained with a carbon abundance of 8.7 dex and $^{12}C/^{13}C \sim 10.1$ returns a nitrogen abundance of 7.1 dex (dotted lines). The solid line corresponds to the observed spectrum. Two alternative plots with long-dash and short-dash are shown with [N/Fe] = ±0.3 from the adopted value.

Table 5: Elemental abundances in CD−27 14351

	Z	solar $log\epsilon^a$	$log\epsilon$	[X/H]	[X/Fe]
C I	6	8.43	8.70±0.20	0.27	2.89
N I	7	7.83	7.10±0.20	-0.73	1.89
Na I	11	6.24	4.89±0.20	-1.35	1.27
Mg I	12	7.60	5.61±0.40	-1.99	0.63
Ca I	20	6.34	4.51±0.18	-1.83	0.79
Ti I	22	4.95	3.25±0.18	-1.70	0.92
Ti II	22	4.95	3.21±0.16	-1.74	0.83
Cr I	24	5.64	2.84±0.17	-2.80	-0.18
Fe I	26	7.50	4.87±0.15	-2.63	-
Fe II	26	7.50	4.93±0.09	-2.57	-
Sr I	38	2.87	2.02±0.20	-0.85	1.77
Sr I*	38	2.87	1.98±0.20	-0.89	1.73
Y II	39	2.21	1.63±0.12	-0.58	1.99
Y II*	39	2.21	1.55±0.20	-0.66	1.91
Ba II	56	2.18	1.40±0.07	-0.78	1.79
Ba II*	56	2.18	1.38±0.20	-0.8	1.77
La II	57	1.10	0.29±0.18	-0.81	1.76
La II*	57	1.10	0.10±0.20	-1.00	1.57
Ce II	58	1.58	1.43±0.30	-0.15	2.63
Nd II	60	1.42	0.11±0.08	-1.31	1.26
Nd II*	60	1.42	−0.05±0.20	-1.47	1.10
Eu II*	63	0.52	−0.40±0.20	-0.92	1.65

[a] Asplund et al. (2009)

* Abundance estimates are from spectral synthesis calculation.

5.4. Fe-peak elements

Two Cr I lines at 5247.57 and 5348.31 Å are used to derive the Cr abundance. Cr shows under abundance with [Cr/Fe] value −0.18. We have detected many Ni lines in the spectrum of CD−27 14351. But none of them are usable for abundance calculation due to distortion and severe line blending.

5.5. Abundances of neutron-capture elements

Abundances of neutron-capture elements are derived by the equivalent width measurements as well as by the spectral synthesis calculations. We have accounted for any possible blending due to other elements in the linelists of the respective lines used for spectral synthesis calculation. The derived abundances along with the error estimates are listed in table 5. Abundance of Sr is derived from the Sr I line at 4607.7 Å. Sr is found to be enhanced with [Sr/Fe] ∼ 1.75. Y also shows an enhancement with [Y/Fe] ∼ 1.95. The spectrum synthesis fits are shown in figure 5. We could not measure any Zr lines in the spectrum of CD−27 14351. Ba abundance calculated by measuring the equivalent widths of Ba II lines at 4934, 6141 and 6496 Å give a [Ba/Fe] value of 1.79. The spectrum synthesis of Ba II line at 6141.713 Å (figure 6) considering the hyperfine splitting contributions from McWilliam (1998) gives [Ba/Fe] ∼ 1.77. We have derived La abundance from spectrum synthesis calculation of La II line at 4921.77 Å considering hyperfine components from Jonsell et al. (2006) which gives [La/Fe] ∼ 1.57. Cerium abundance derived from two Ce II lines at 4460.2 and 4527.3 Å indicates a large enhancement of Ce with [Ce/Fe] ∼ 2.63. Nd abundance calculated by the equivalent width measurement of four Nd II lines gives [Nd/Fe] ∼ 1.26. We have also derived the Nd abundance by spectral synthesis calculation of Nd II line at 5212.3 Å (figure 5); this gives a value of 1.1 for [Nd/Fe]. We have derived Eu abundance from Eu II line at 6645.130 Å by considering the hyperfine components from Worley et al. (2013). Although the right wing of this Eu line is found to be blended with Fe I line at 6645.36 Å and a Tb I line at 6645.37 Å we could get a proper fit for the left wing with the adopted Eu abundance of −0.40 dex (figure 6). The adopted Eu abundance gives [Eu/Fe] ∼ 1.65. We could not detect Eu lines at 4129 and 6437 Å.

Table 6: Abundance ratios of light and heavy s-process elements

Star Name	[Fe/H]	[ls/Fe]	[hs/Fe]	[hs/ls]
CD−27 14351	−2.62	1.82	1.77	−0.05

[ls/Fe] and [hs/Fe] are calculated using the abundance values obtained from spectral synthesis calculations as given in table 5.

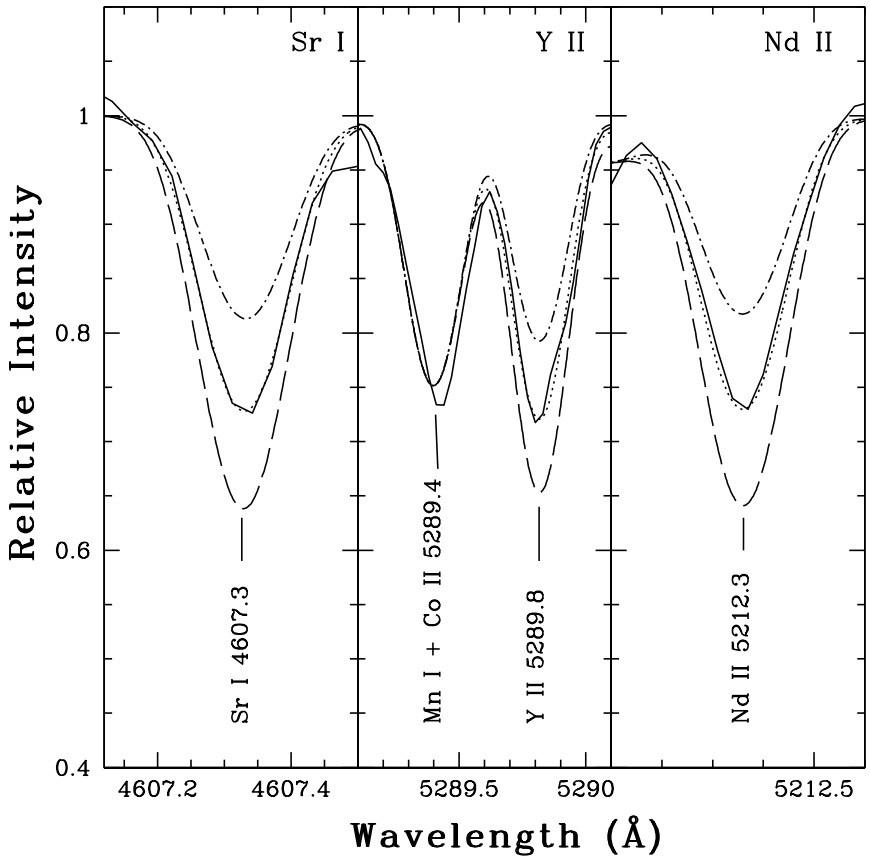

Fig. 5.— Spectral-synthesis fits of Sr I line at 4607.3 Å, Y II line at 5289.8 Å and Nd II line at 5212.3 Å are shown. The dotted lines indicate the synthesized spectra and the solid lines indicate the observed line profiles. Two alternative synthetic spectra for [X/Fe] = +0.3 (long-dashed line) and [X/Fe] = −0.3 (short-dashed line) from the adopted value are shown to demonstrate the sensitivity of the line strength to the abundances.

Table 7: Abundance Uncertainties

Star	Standard error	δT_{eff} ±100K	δ log g ±0.1	$\delta\xi$ ±0.3 km/s	Total Uncertainty
CD−27 14351	0.15	0.08	0.01	0.09	0.17

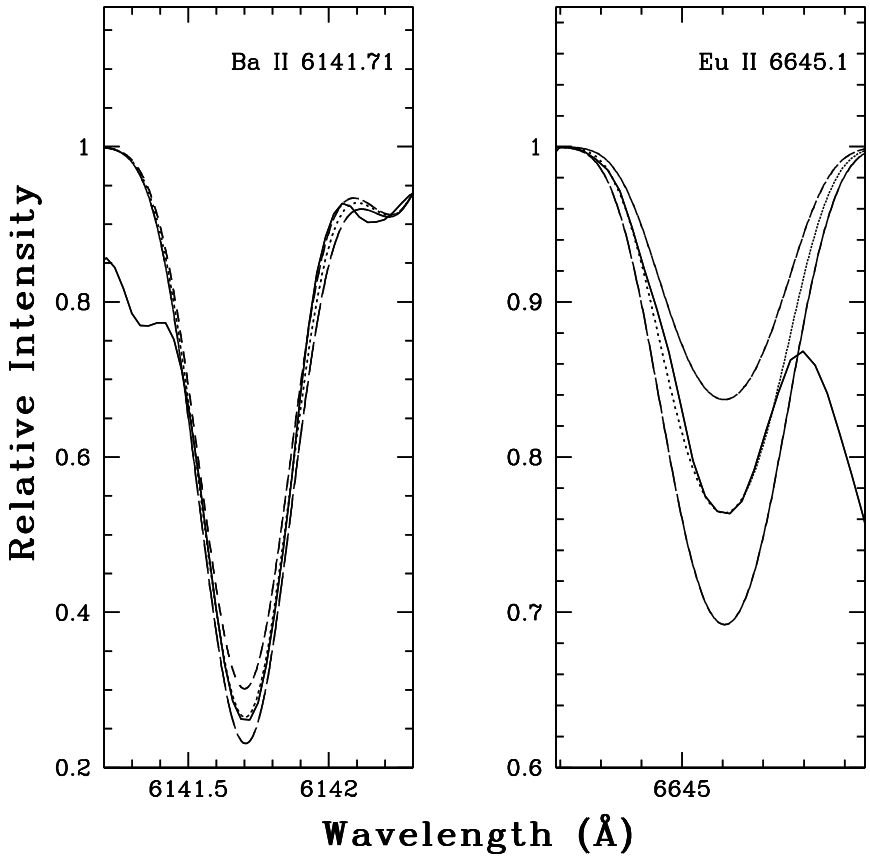

Fig. 6.— Spectral-synthesis fits of Ba II line at 6141.71 Å and Eu II line at 6645 Å. In both the panels the dotted lines indicate the synthesized spectra and the solid lines indicate the observed line profiles. Two alternative synthetic spectra for [X/Fe] = +0.3 (long-dashed line) and [X/Fe] = −0.3 (short-dashed line) from the adopted value are shown to demonstrate the sensitivity of the line strength to the abundances.

6. Uncertainty in elemental abundance

We have derived the uncertinities in elemental abundance estimates by varying the stellar atmospheric parameters T_{eff}, log g and microturbulence in the model atmosphere. We have calculated the uncertainty due to temperature by varying the temperatures by ± 100 K and recalculated the Fe abundance. Similarly by varying the log g value by ± 0.1 and micro turbulent velocity by ± 0.1 km s^{-1}, we have calculated the corresponding uncertainties in abundances due to these changes. These values, along with the standard error are listed in table 7. The total uncertainty is calculated using the standard equation of error calculations

$$E_r = \sqrt{{E_{r1}}^2 + {E_{r2}}^2 + {E_{r3}}^2 + {E_{r4}}^2} \quad (1)$$

We have assumed this value as the minimum error in the derived abundances.

7. Conclusions

A detailed chemical composition study of CD−27 14351 based on a high resolution FEROS spectrum revealed many important features of this object. The object is characterized by a large enhancement in carbon; a similar enhancement in nitrogen is also evident from our analysis. Such high abundances of carbon and nitrogen are also seen in other CEMP stars (figure 7); these two elements however show a large scatter with respect to metallicity. The α-elements Mg, Ca, Ti and Fe-peak element Cr show similar abundances as are generally noticed in CEMP stars; the high abundance of Na is also a common feature of many CEMP stars (figure 8). A comparison of our estimated abundance ratios of neutron-capture elements with those of Allen et al. (2012); Goswami et al. (2006); Goswami & Aoki (2010); Goswami et al. (2016) and Masseron et al. (2010), for CEMP stars is shown in figure 9. A similar comparison of the neutron-capture elements abundance ratios observed in CD−27 14351 with their counterparts observed in CEMP-s and CEMP-r/s stars alone from Jonsell et al. (2006) clearly shows that Sr, Y and Ce are highly enhanced whereas Ba, La and Eu are similarly enhanced as seen in the case of CEMP-r/s stars. Large enhancement of s-process elements along with the enhancement in Mg indicates the operation of ^{22}Ne(α,n)^{25}Mg as the main neutron source in CEMP-r/s stars (Masseron et al. 2010). As suggested by Gallino et al. (1998) and Goriely & Mowlavi (2000) neutron density associated with this reaction favours production of the s-process element Ce and also the r-process element Eu. Highly enhanced abundances of these two elements observed in this star support this idea. However, Goriely & Siess (2005) suggest that a −ve value of [La/Ce] indicates the operation of ^{13}C(α,n)^{16}O reaction, and, a value of [La/Ce] within the range 0.2 to 0.4 indicates the operation of ^{22}Ne(α,n)^{25}Mg reaction. Our estimated [La/Ce] = −1.06 would therefore imply the reaction ^{13}C(α,n)^{16}O to be the main

source of neutrons. Estimated [Ba/Eu] (= 0.12) indicates that the object can be placed in CEMP-r/s group. Although the binarity among CEMP-s stars are well known, there are a very few studies (e.g. Abate et al. (2016)) focussed on the orbital properties of CEMP-r/s stars. Inspite of several efforts in literature the origin of CEMP-r/s stars still remains far from clearly understood. However in future, it would be worthwhile to investigate if the observed abundance pattern in CD −27 14351 could arise from nucleosynthesis of i-process. Our observational results are expected to help constrain theoretical modelling providing insight and better understanding of the origin of such objects.

Acknowledgements
AG, the PI of the HCT observing proposal and DK would like to thank the staff at IAO and at the remote control station at CREST, Hosakote, for assistance during the observations. This work made use of the SIMBAD astronomical data base, operated at CDS, Strasbourg, France, and the NASA ADS, USA. Funding from the DST project SB/S2/HEP-010/2013 is gratefully acknowledged. This work was partly supported by the European Union FP7 programme through ERC grant number 320360.

REFERENCES

Abate, C., Stancliffe, R. J., & Liu, Z.-W. 2016, A&A, 587, A50

Allen, D. M., Ryan, S. G., Rossi, S., Beers, T. C., & Tsangarides, S. A. 2012, A&A, 548, A34

Alonso, A., Arribas, S., & Martínez-Roger, C. 1999, A&AS, 139, 335

Alonso, A., Arribas, S., & Martínez-Roger, C. 2001, A&A, 376, 1039

Andersen, T. & Petkov, A. P. 1975, A&A, 45, 237

Aoki, W., Beers, T. C., Christlieb, N., et al. 2007, ApJ, 655, 492

Aoki, W., Beers, T. C., Sivarani, T., et al. 2008, ApJ, 678, 1351

Aoki, W., Norris, J. E., Ryan, S. G., Beers, T. C., & Ando, H. 2002a, ApJ, 576, L141

Aoki, W., Norris, J. E., Ryan, S. G., Beers, T. C., & Ando, H. 2002b, ApJ, 567, 1166

Asplund, M., Grevesse, N., Sauval, A. J., & Scott, P. 2009, ARA&A, 47, 481

Barbuy, B., Spite, M., Spite, F., et al. 2005, A&A, 429, 1031

Baumueller, D. & Gehren, T. 1997, A&A, 325, 1088

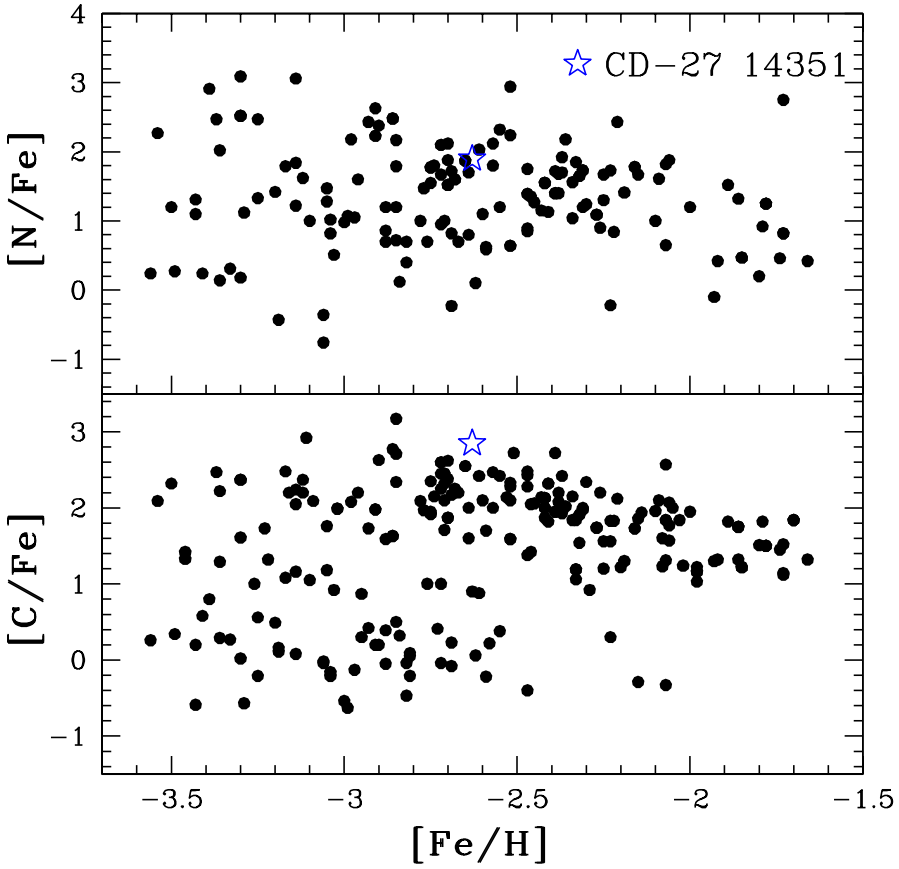

Fig. 7.— This figure shows a comparison of the [C/Fe] (lower panel) and [N/Fe] (upper panel) values observed in CD−27 14351 (shown with a star symbol in both the panels) with their counterparts (solid circles) in CEMP stars from literature (e.g., Masseron et al. (2010)).

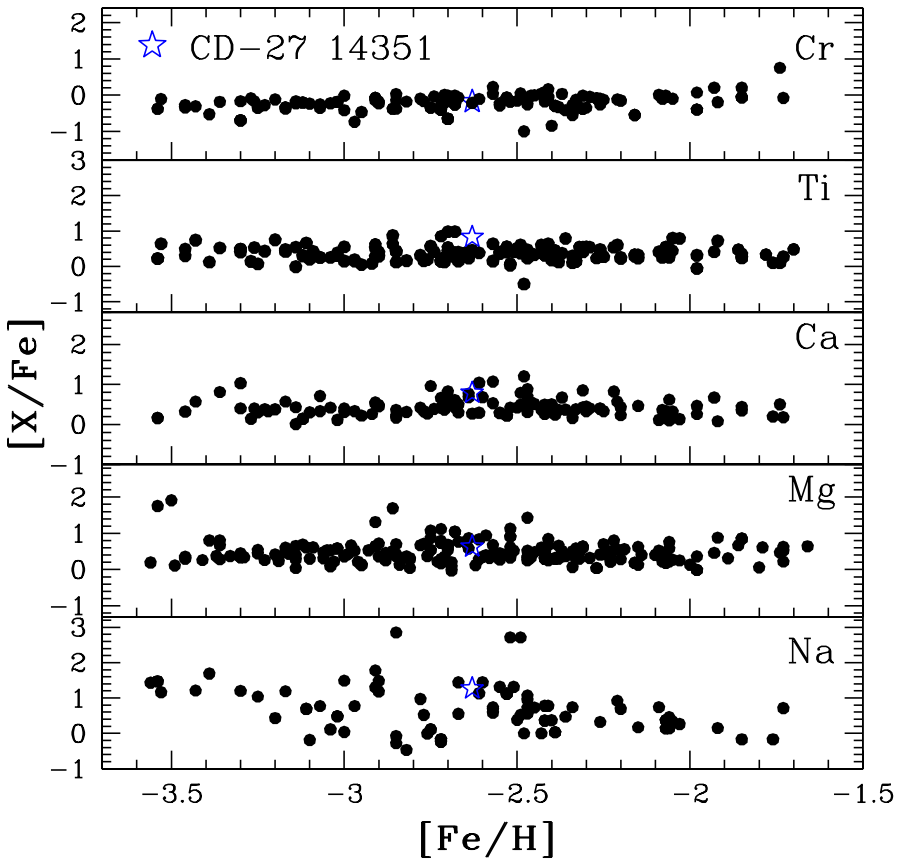

Fig. 8.— Comparison of the observed light element abundances of CD−27 14351 (indicated by a star symbol) with their counterparts in CEMP stars available in literature (i.e., Allen et al. (2012); Goswami et al. (2006); Goswami & Aoki (2010); Goswami et al. (2016); Masseron et al. (2010)).

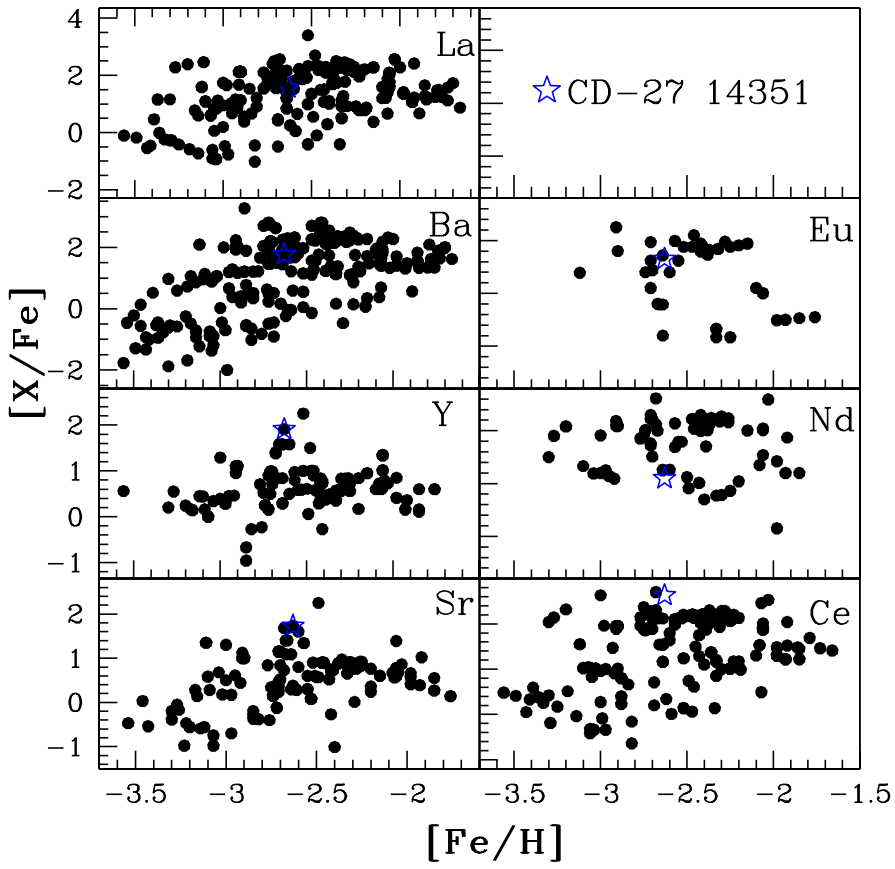

Fig. 9.— Comparison of the observed heavy element abundances in CD−27 14351 (indicated by a star symbol) with their counterparts in CEMP stars available in literature (i.e., Allen et al. (2012); Goswami et al. (2006); Goswami & Aoki (2010); Goswami et al. (2016); Masseron et al. (2010)).

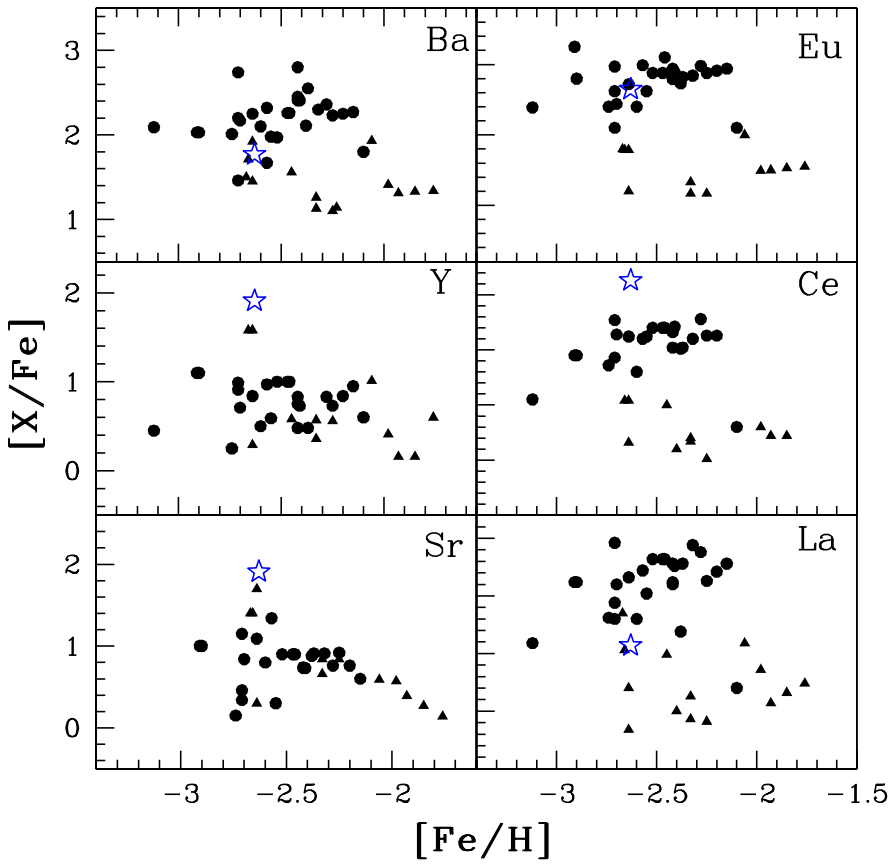

Fig. 10.— comparison of the observed heavy element abundances in CD−27 14351 (indicated by a star symbol) with values from other CEMP-r/s (solid circle) and CEMP-s stars (solid triangle) from Jonsell et al. (2006).

Beers, T. C. & Christlieb, N. 2005, ARA&A, 43, 531

Biemont, E., Karner, C., Meyer, G., Traeger, F., & Zu Putlitz, G. 1982, A&A, 107, 166

Bridges, J. M. & Kornblith, R. L. 1974, ApJ, 192, 793

Brooke, J. S. A., Bernath, P. F., Western, C. M., et al. 2013, in 68th International Symposium on Molecular Spectroscopy, ERD02

Corliss, C. H. & Bozman, W. R. 1962, Experimental transition probabilities for spectral lines of seventy elements; derived from the NBS Tables of spectral-line intensities

Cowley, C. R. & Corliss, C. H. 1983, MNRAS, 203, 651

Fuhr, J. R., Martin, G. A., & Wiese, W. L. 1988, Journal of Physical and Chemical Reference Data, 17

Gallino, R., Arlandini, C., Busso, M., et al. 1998, ApJ, 497, 388

Goriely, S. & Mowlavi, N. 2000, A&A, 362, 599

Goriely, S. & Siess, L. 2005, in IAU Symposium, Vol. 228, From Lithium to Uranium: Elemental Tracers of Early Cosmic Evolution, ed. V. Hill, P. Francois, & F. Primas, 451–460

Goswami, A. 2005, MNRAS, 359, 531

Goswami, A. & Aoki, W. 2010, MNRAS, 404, 253

Goswami, A., Aoki, W., Beers, T. C., et al. 2006, MNRAS, 372, 343

Goswami, A., Aoki, W., & Karinkuzhi, D. 2016, MNRAS, 455, 402

Hampel, M., Stancliffe, R. J., Lugaro, M., & Meyer, B. S. 2016, ArXiv e-prints

Hannaford, P., Lowe, R. M., Grevesse, N., Biemont, E., & Whaling, W. 1982, ApJ, 261, 736

Johnson, J. A. 2002, ApJS, 139, 219

Jonsell, K., Barklem, P. S., Gustafsson, B., et al. 2006, A&A, 451, 651

Kurucz, R. L. 1988, in Astrophysics and Space Science Library, Vol. 138, IAU Colloq. 94: Physics of Formation of FE II Lines Outside LTE, ed. R. Viotti, A. Vittone, & M. Friedjung, 41

Kurucz, R. L. & Peytremann, E. 1975, SAO Special Report, 362

Laughlin, C. & Victor, G. A. 1974, ApJ, 192, 551

Lincke, R. & Ziegenbein, B. 1971, Zeitschrift fur Physik, 241, 369

Martin, G. A., Fuhr, J. R., & Wiese, W. L. 1988, Atomic transition probabilities. Scandium through Manganese

Masseron, T., Johnson, J. A., Plez, B., et al. 2010, A&A, 509, A93

Masseron, T., Plez, B., Van Eck, S., et al. 2014, A&A, 571, A47

McEachran, R. P. & Cohen, M. 1971, J. Quant. Spec. Radiat. Transf., 11, 1819

McWilliam, A. 1998, AJ, 115, 1640

Meggers, W. F., Corliss, C. H., & Scribner, B. F. 1975, Tables of spectral-line intensities. Part I, II_- arranged by elements.

Miles, B. M. & Wiese, W. L. 1969, Atomic Data, 1, 1

Qian, Y.-Z. & Wasserburg, G. J. 2003, ApJ, 588, 1099

Ram, R. S., Brooke, J. S. A., Bernath, P. F., Sneden, C., & Lucatello, S. 2014, ApJS, 211, 5

Sneden, C., Lucatello, S., Ram, R. S., Brooke, J. S. A., & Bernath, P. 2014, ApJS, 214, 26

Sneden, C. A. 1973, PhD thesis, THE UNIVERSITY OF TEXAS AT AUSTIN.

Wanajo, S., Nomoto, K., Iwamoto, N., Ishimaru, Y., & Beers, T. C. 2006, ApJ, 636, 842

Ward, L., Vogel, O., Arnesen, A., Hallin, R., & Wännström, A. 1985, Phys. Scr, 31, 161

Worley, C. C., Hill, V., Sobeck, J., & Carretta, E. 2013, A&A, 553, A47

Zijlstra, A. A. 2004, MNRAS, 348, L23

This preprint was prepared with the AAS LaTeX macros v5.2.